The effect of mountain uplift on eastern boundary currents and upwelling systems

Gerlinde Jung[1,2], Matthias Prange[1,2]

[1]MARUM - Center for Marine Environmental Sciences, University of Bremen, 28334 Bremen, Germany
5 [2] Faculty of Geosciences, University of Bremen, 28334 Bremen, Germany

Correspondence to: Gerlinde Jung (gjung@marum.de)

Abstract. All major mountain ranges are assumed to have been subject to increased uplifting processes during the late Miocene and Pliocene. Previous work has demonstrated that African uplift is an important element to explain Benguela upper-ocean cooling in the late Miocene/Pliocene. According to proxy records, a surface ocean cooling also occurred in
10 other Eastern Boundary upwelling regions during the late Neogene. Here we investigate a set of sensitivity experiments altering topography in major mountain regions (Andes, North American Cordillera and South/East African mountains) separately with regard to the potential impact on the intensity of near-coastal low-level winds, Ekman transport and Ekman pumping as well as upper-ocean cooling. The simulations show that mountain uplift is important for upper-ocean temperature evolution in the area of Eastern Boundary Currents. The impact is primarily on the atmospheric circulation
15 which is then acting on upper-ocean temperatures through changes in strengths of upwelling, horizontal heat advection and surface heat fluxes. Different atmosphere-ocean feedbacks additionally alter the sea surface temperature response to uplift. The relative importance of the different feedback mechanisms depends on the region, but is most likely also influenced by model and model resolution.

1 Introduction

20 Eastern Boundary Upwelling Systems (EBUSs) are found off the West coasts of all continents bordering the Atlantic and Pacific Ocean. These upwelling systems are characterized by high biological activity and the world's richest fishing grounds due to the upwelling of cool subsurface nutrient-rich waters (Garcia-Reyes and Largier, 2012). The upwelling systems also influence climatic patterns of the land region because local sea surface temperature (SST) is strongly linked to rainfall distribution (e.g. Rouault et al., 2003).

25 Coastal upwelling is mainly occurring as a response to Ekman transport by alongshore winds and due to wind-stress-curl-driven ocean-surface divergence offshore (in this study we refer to both processes as Ekman pumping and define upward pumping, sometimes called "Ekman suction", to be positive). Furthermore, a strong feedback exists between near-coastal winds and SST (Nicholson, 2010;Garcia-Reyes and Largier, 2012), since SST has a strong influence on the wind field through atmospheric boundary layer stability and dynamics. The major Eastern Boundary Currents are formed by

equatorward directed winds at the eastern flanks of the Subtropical Gyres. Due to the presence of the coastline the associated winds induce an Ekman-driven upwelling near the coast (Chavez and Messie, 2009). Apart from coastal and large-scale winds, also offshore and remote ocean conditions (e.g. the strength and depth of the thermocline) influence upwelling activity (Garcia-Reyes and Largier, 2012). The characteristics of EBUSs are also determined by water column stratification,

5   coastal topography and latitudinal position (i.e. influencing seasonality and through the latitudinal dependence of the Coriolis parameter) (Chavez and Messie, 2009). Additionally, the size of the ocean basin is important, where smaller basins, like the Atlantic are less influenced by thermocline perturbations than the larger Pacific Ocean (Chavez and Messie, 2009).

Proxy data from all major EBUSs of the world indicate a strengthening of upwelling intensity during the late Neogene (Dekens et al., 2007). The South American (Strecker et al., 2007), as well as North American and African continent were

10   situated at approximately the same geographic location throughout most of the Neogene (Scotese, 1998), hence an upwelling intensification through continental shifts is not a very likely scenario. Different proxy studies indicate that all major near-coastal mountain ranges showed significant uplift during the period of upwelling intensification (see below). As mountains act in enhancing the land-ocean temperature gradient, mountain uplift has an impact on thermal wind and baroclinity in the atmospheric boundary layer. Therefore, topographic uplift of, especially, the coastal regions might well serve to intensify

15   upwelling in EBUSs, as was demonstrated by Jung et al. (2014) for the Benguela upwelling system.

In the present study we use a coupled ocean-atmosphere general circulation model (GCM) including a dynamic vegetation module. Different model experiments were performed altering topography of East and Southern Africa, the Andes, and the North American Cordillera separately. In these sensitivity experiments topography is the only boundary condition that is altered. Therefore this study aims at understanding the role of continental-scale topography uplift in Neogene upwelling

20   intensification in three major Eastern Boundary upwelling systems. We compare the responses of 1) the Humboldt Current and Upwelling System to Andean uplift, 2) the California Upwelling System to an uplift of the North American Cordillera, and 3) the Benguela Upwelling System to African uplift (as discussed in Jung et al. (2014)).

2 Eastern Boundary Upwelling Systems

2.1 Modern Eastern Boundary Upwelling Systems

25   The Benguela Upwelling System is confined by the Angola-Benguela-Front to the North and by the Agulhas Current to the South. The upwelling cell at Lüderitz persists all year, whereas North of Lüderitz the main upwelling season is in austral winter and South of Lüderitz in austral summer (Hutchings et al., 2009). The main zone of year-round upwelling reaches from ~15°S to ~30°S (Chavez and Messie, 2009), and the most important driver of Benguela upwelling is the wind stress of the low-level Benguela Jet (Nicholson, 2010).

30   The California upwelling region contains several upwelling regimes and extends from the North Pacific current to off Mexico. The zone of strongest upwelling lies between ~34°N and ~44°N (Chavez and Messie, 2009). It is forced by the North Pacific High, which is especially strong during boreal summer season. California upwelling is characterized by a

strong seasonality with the main upwelling season occurring from April to June with strong upwelling favourable winds of the low-level jet (Garcia-Reyes and Largier, 2012). The formation and dynamics of the coastal jet along the California coast has extensively been studied (e.g. Holt, 1996;Doyle, 1997;Burk and Thompson, 1996;Parish, 2000). In winter the Aleutian Low is dominantly strong, leading to winds directed to the North and hence favouring downwelling in most of the area. Only

5 South of about Cape Mendicino there is a year-round, but weak upwelling zone (Checkley and Barth, 2009).

The EBUS of the South Pacific Ocean in the region of the Humboldt Current (also called the Peru Current) is referred to as the Humboldt (or Peru-Chile) Upwelling System. Coastal upwelling is quasi-permanent off Peru and northern Chile, but shows a strong seasonality south of 30°S with maximum upwelling-favourable winds in austral summer (Montecino and Lange, 2009). Only Peru upwelling shows a year-round activity between ~4°S to ~16°S (Chavez and Messie, 2009), but it is

10 periodically disrupted by the El Nino Southern Oscillation (ENSO). The characteristics of the upwelling system are set by wind strength related to the South Pacific Anticyclone and the effects of coastal topography on the alongshore wind. The coastal jet off Chile at the eastern flank of the South Pacific Anticyclone (Munoz and Garreaud, 2005;Garreaud and Munoz, 2005) plays also an important role in the feedback mechanism regarding SST conditions and upwelling activity (Renault et al., 2009).

2.2 Global upwelling intensification during the Neogen

Paleo-climatological proxy records off the Western coasts of the continents indicate a cooling for all EBUSs at least since the Pliocene. The strongest cooling is found for the Benguela (-9.3°C) and California (-8.8°C) Upwelling Systems, whereas a weaker cooling (-2.9°C) is found for the Humboldt (Peru and Chile) upwelling region (Dekens et al., 2007).

Benguela upwelling is suggested to have initiated and successively intensified since ~ 14 Ma (Rommerskirchen et al.,
20 2011;Marlow et al., 2000). The Miocene initiation of Benguela upwelling is also assumed to be related to a northward migration of the Angola-Benguela front (Bergh et al., 2018). This is also evident in vegetation changes that indicate an aridification of the adjacent land of Southern Africa (Hoetzel et al., 2015;Dupont et al., 2013).

The Humboldt Current, as well as the Humboldt Upwelling System are suggested to have been active since the early Cenozoic (Keller et al., 1997). Also aridity in the Atacama desert already existed prior to the Miocene/Pliocene (Clarke,
25 2006). Nevertheless, aridity in the Southern Central Andes is a function of the latitudinal position of the cold upwelling zone along the Chilean coast (Strecker et al., 2007) and hence is influenced by upwelling intensity. According to proxy records the Peru Upwelling System showed a gradual cooling since about 4 Ma (Dekens et al., 2007), whereas the California Upwelling System intensification began in the early middle Miocene (White et al., 1992).

3 Uplift histories

30 All major mountain areas of the world were subject to uplift in the late Neogene. The related processes are likely connected to the activity of two superplumes (Potter and Szatmari, 2009). But studies on the timings of uplift and estimates of uplift

rates are rarely in consensus and paleoaltimetry based on stable isotope methods might overestimate rapid uplift, as has been demonstrated in a study for the Andes by Ehlers and Poulsen (2009). Hence the uplift histories of the world's major mountain ranges are still a matter of debate

3.1 Africa

The southern and eastern African plateaus belong to the African superswell (Nyblade and Robinson, 1994). This topographic anomaly is considered to have developed since the early Miocene (Seranne and Anka, 2005) and it was subject to strong tectonic uplift during the past 30 Myr with a maximum rate in the late Pliocene and early Pleistocene (Moucha and Forte, 2011;Pik, 2011). For Southern Africa, proxy evidence suggests that most of the landscape has been formed during the Neogene, with regional differences ranging from an initiation of uplift in the Namibian region around 30 Ma to more recent uplift intensifications of 10 Ma for the South African swell and the Bié plateau (Roberts and White, 2010). East African uplift can also be attributed to the uplift of rift shoulders that are superimposed on the swell due to volcanism and rifting. Recently evidence for a rather synchronous beginning of uplift of the Eastern and Western parts of East Africa around 25 Ma was found (Roberts et al., 2012), in contrast to a later uplift of the Western part around 5 Ma as previously assumed (Sepulchre et al., 2006).

3.2 Andes

Late Miocene climatic changes in the Southern Central Andes, with increasingly humid conditions east of the Puna and the development of hyperarid conditions at the Western flanks of the Southern Central Andes is in contrast to the expected aridity due to late Miocene global cooling and hence points to a tectonic origin (Strecker et al., 2007). The Precordillera in the Southern Atacama Desert is suggested to have attained an elevation of at least 3000 m already in the early Oligocene, prior to the uplift ot the Altiplano (Bissig and Riquelme, 2010). A recent study of pollen records from western equatorial South America indicated that the Central Andes were already at a reasonable height for blocking air flow and influencing precipitation pattern by the middle Miocene (Grimmer et al., 2018). Most of the Andean uplift is supposed to have occurred during the middle and late Miocene (Potter and Szatmari, 2009). It is suggested that exhumation in the Central Andes moved eastward, beginning in the Eastern Cordillera at ~50-15 Ma, reaching about 75% of present-day elevation in the Bolivian Andes at ~15-11 Ma (Barnes et al., 2012). According to Gregory-Wodzicki (2000), the Central Andean Cordillera reached about a third of its present altitude 20 Ma ago and about 50% of present elevation by 10.7 Ma implying a magnitude of uplift of around 2300-3400 m since the late Miocene. For the Colombian Andes rapid uplift between 2 and 5 Ma was suggested (Gregory-Wodzicki, 2000). These timings of uplift of the Central Andes are in agreement with a recorded change in South American seasonality indicating a southward deflection of the South American low-level jet at around 8-9 Ma (Mulch et al., 2010) and with the onset of humid conditions on the Eastern side of the Southern Central Andes in the late Miocene (Strecker et al., 2007). Miocene surface uplift is also documented for the Southern Patagonian Andes (Blisniuk et al., 2005).

Uplift of the Bolivian Altiplano was estimated as 2.5 to 3.5 km between about 10 and 6 Ma (Ghosh et al., 2006;Garzione et al., 2006)

3.3 North American Cordillera

The North American Cordillera comprises different mountain and plateau areas as the Sierra Nevada, the Rocky Mountains,
the High Plains and the Colorado plateau. These have distinct uplift histories with also high levels of uncertainty. Parts of the
North American Cordillera were already at a high elevation since the Early Cenozoic (Foster et al., 2010, and references
therein). Nevertheless major uplift events took also place from the middle Miocene on. Uplift in the Rocky Mountains
initiated in the middle Miocene, whereas the northern coastal mountains of Canada show a steady rise since 10 Ma (Potter
and Szatmari, 2009). The coastal ranges of central and southern California are still rising. They were subject to deformation
in the late Miocene, as well as to folding and uplift that initiated around 3.5 Ma (Page et al., 1999;Montgomery, 1993).

4 Methods

4.1 Model Description

The model simulations were performed with the National Center for Atmospheric Research (NCAR) Community Climate
System Model Version 3 (CCSM3) (Collins et al., 2006). The model is run in a fully coupled mode, including the four
components atmosphere, land, ocean, and sea ice. The atmospheric component (CAM3) and the land surface model (CLM3)
are run at a horizontal resolution of ~1.4° (T85); the atmosphere is discretized with 26 vertical layers. The ocean (POP) and
sea-ice models (CSIM) are run with a variable grid resolution of 1.125° in zonal direction and roughly 0.5° in meridional
direction, with a refinement down to 0.3° towards the equator. The ocean model uses 40 levels in the vertical. The land
model includes a dynamical global vegetation model (DGVM) (Levis et al., 2004;Bonan et al., 2003) and improved
parameterizations for canopy interception and soil evaporation (Oleson et al., 2008;Handiani et al., 2013;Rachmayani et al.,
2015). This enables not only the direct simulation of vegetation coverage response to climatic conditions, but also the
consideration of biogeophysical feedbacks between climate and vegetation.

4.2 Experimental Design

Three model experiments were performed. A control simulation (CTRL), as in Jung et al. (2014) which is also described in
detail further down, was run using present-day topography. Three sensitivity studies were performed that are identical to
CTRL, except that topography was lowered to 50% of the present-day altitude for Eastern and Southern Africa (AF), for the
Andes (AND), and for the North American Cordillera (NA), respectively (Figure 1).
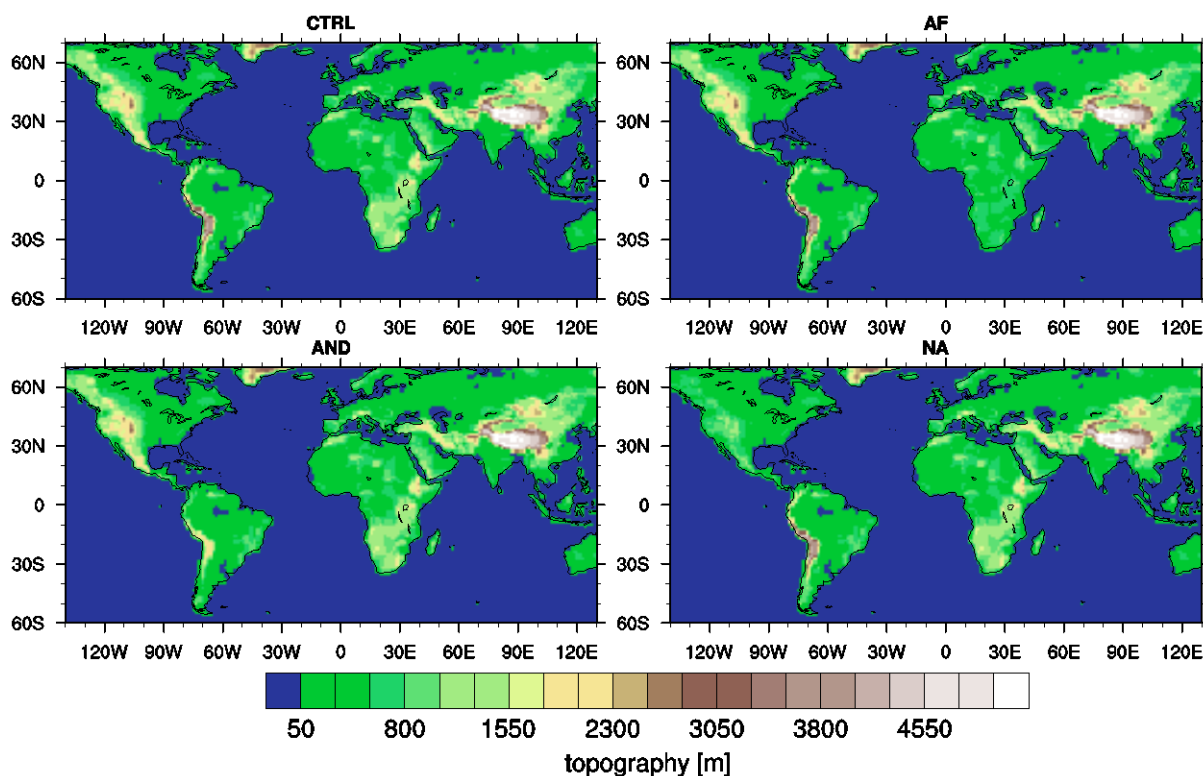
Fig. 1: Model topographies of the different experiments: present day topography (CTRL)(upper left), South and East African topography 50% of CTRL (AF)(upper right), Andean topography 50% of CTRL (AND)(lower left), North American Cordilleran topography 50% of CTRL (NA)(lower right).

5   The boundary conditions for the control run (CTRL) are present-day with respect to geography, topography and pre-industrial with respect to greenhouse gases, ozone concentrations, sulphate and carbonaceous aerosols (Braconnot et al., 2007). Assuming pre-desert conditions, the effect of dust aerosols on radiative transfer was set to zero and soil texture and colour were adapted to represent loam in the Sahara. To avoid extreme insolation forcing, the orbital parameters were set to represent average values over the period of 2-10 Myr with an eccentricity of 0.027 and an obliquity of 23.25°. The perihelion

was set to autumn (359.47°). In comparison to an identical setup, but with preindustrial orbital configuration, our control simulation is characterized by stronger insolation in the northern hemisphere in summer, and weaker insolation during winter, which leads to an increase in seasonality, which is most pronounced in the northern hemisphere. The control run was started from a spun-up preindustrial simulation of 500 years obtained from NCAR and run for another 600 years. The

5   experiments were branched off from the control run at year 301 and run for another 300 years. It was demonstrated by Jung et al. (2014, Supplementary Information) that the spinup period was sufficient to get the upper ocean in equilibrium. Also the vegetation cover was in equilibrium after the spinup.

All model outputs shown in the following section are averages over a period of 100 years. Differences in the model results section are defined, indicating the anomaly of the control simulation (present-day topography) with respect to the experiment

10   with lowered topography (CTRL minus AF, CTRL minus AND, and CTRL minus NA respectively). Hence the presented results show the simulated response of the variables to mountain uplift.

5 Results

5.1 Evaluation of upwelling velocities in the control run

For an evaluation of the models' representation of upwelling activity, in the following, the vertical oceanic velocities of all

15   regions are compared to observations, or high resolution modelling results, regarding seasonality and magnitude. Even though the boundary conditions of our control run are not exactly present-day (see above), a qualitative comparison is meaningful.

As discussed in Jung et al. (2014, supplementary information, Supplementary Figure 4) upwelling location and seasonality are correctly simulated for the Benguela region, but the magnitude of upwelling velocity is underestimated.

20   For the California upwelling region (Figure 2) the position of the main upwelling zone matches well with the observations (34-44°N according to Chavez and Messie (2009)). As in Chavez and Messie (2009), upwelling does not occur year-round, but only from spring to summer. In Southern California, where upwelling is weaker, upwelling velocities range from a maximum of 2.5 +-1.3 m d^{-1} in May to a minimum of 0.5+-0.6 m d^{-1} in January (Haskell et al., 2015a). Peak summer vertical velocities of about 10 m d^{-1} were estimated for central Californian upwelling by (Pickett and Paduan, 2003). Hence, with

25   values mostly below 1 m d^{-1}, upwelling velocities in the CCSM3 simulations are underestimated despite showing the correct seasonality.
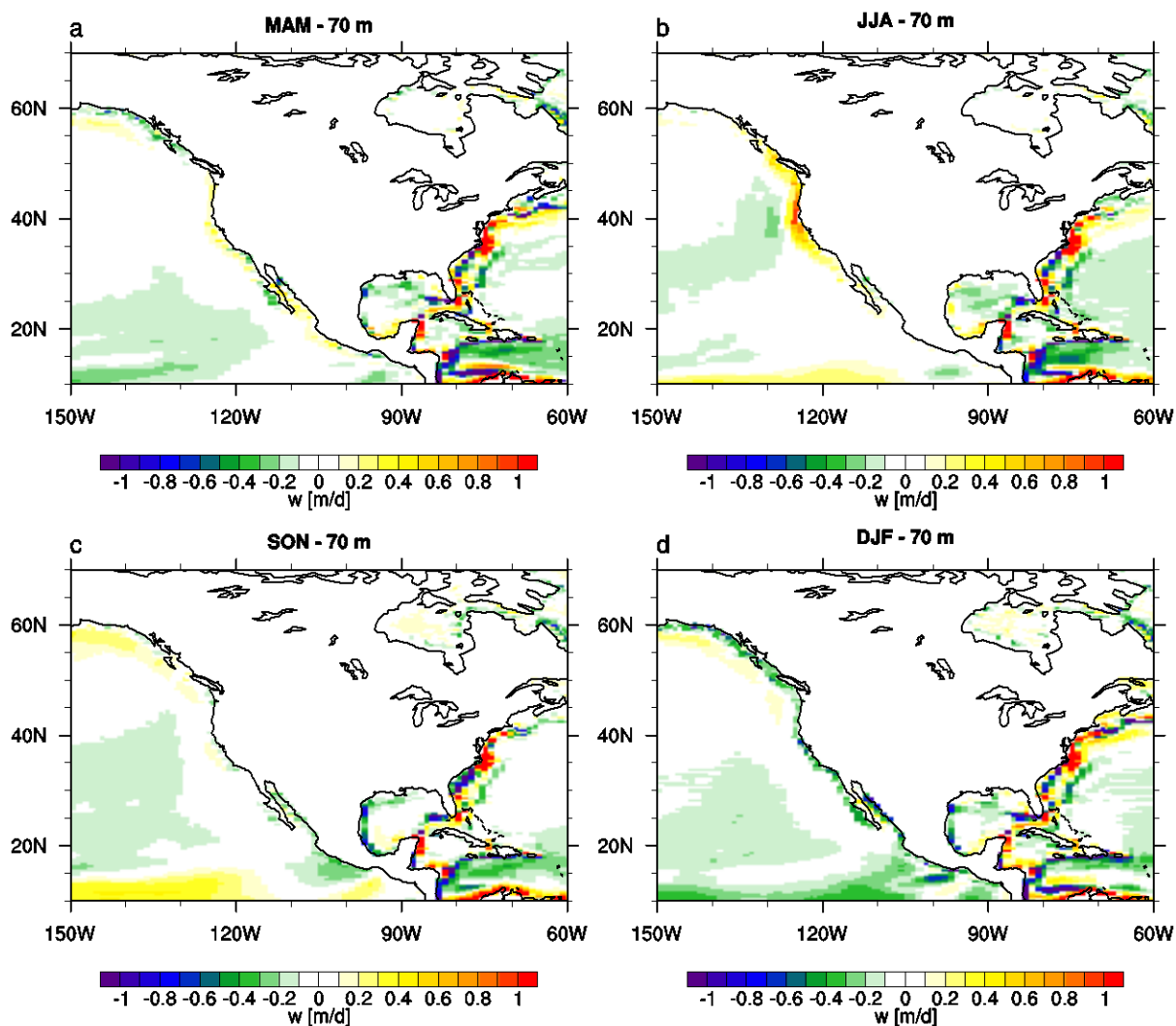
Fig 2: Vertical velocity [m d⁻¹] at a depth of 70m in the control run (CTRL) for MAM (a), JJA (b), SON (c), DJF (d). Positive (negative) values denote upward (downward) motion.
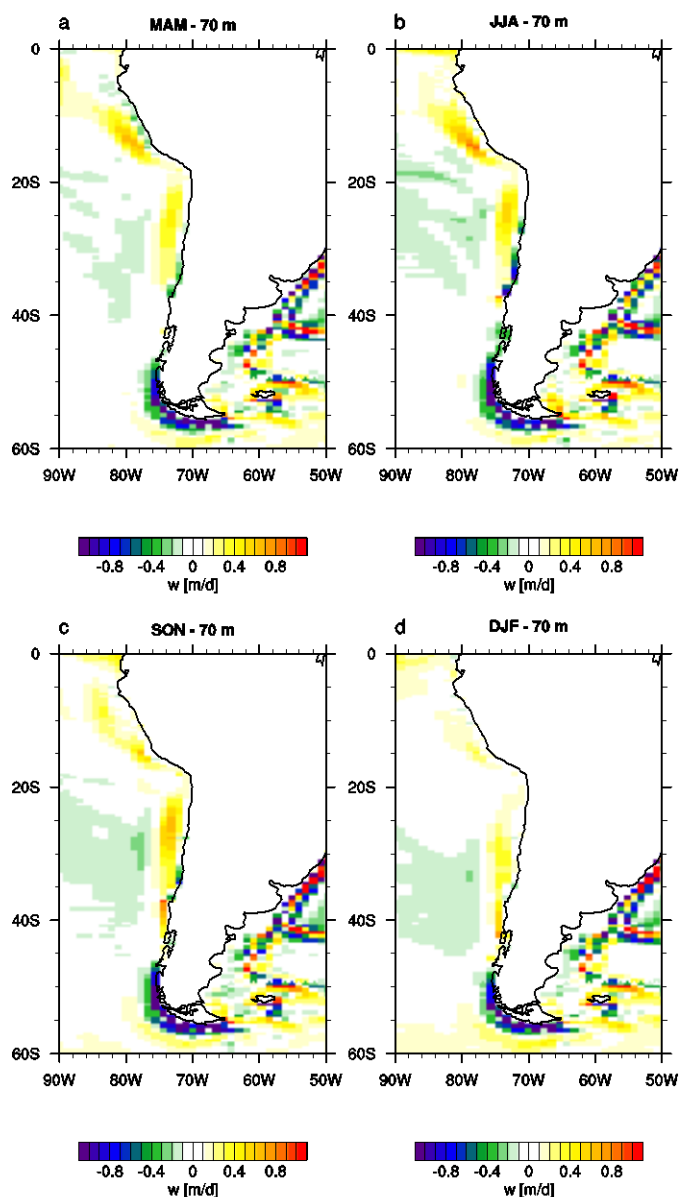
Fig 3: Vertical velocity [m d⁻¹] at a depth of 70m in the control run (CTRL) for MAM (a), JJA (b), SON (c), DJF (d).

Regarding the Humboldt upwelling region, a comparison of our model results (Figure 3) to higher resolved model results of Belmadani et al. (2014), using a GCM of variable resolution down to 0.5° over the region of interest, shows reasonably good agreement. Based on observations, upwelling velocities of the eastern tropical South Pacific range from ~ 0.0 to 1.1 m d⁻¹, depending on location and season (Haskell et al., 2015b). Therefore our model results compare well with ~0.5 m d⁻¹ (up to 0.8 m d⁻¹ during JJA in the Peru upwelling region).

Even though upwelling is underestimated in all areas, representation of upwelling is sufficient in the chosen model resolution to draw some conclusions regarding the posed scientific question.

5.2 Response to mountain uplift

5.2.1 Surface wind and Ekman pumping

5   For the Benguela region (Figure 4), as well as for the California upwelling region (Figure 5) a clear intensification of low-level winds and Ekman pumping velocities is simulated in our experiments upon uplift.
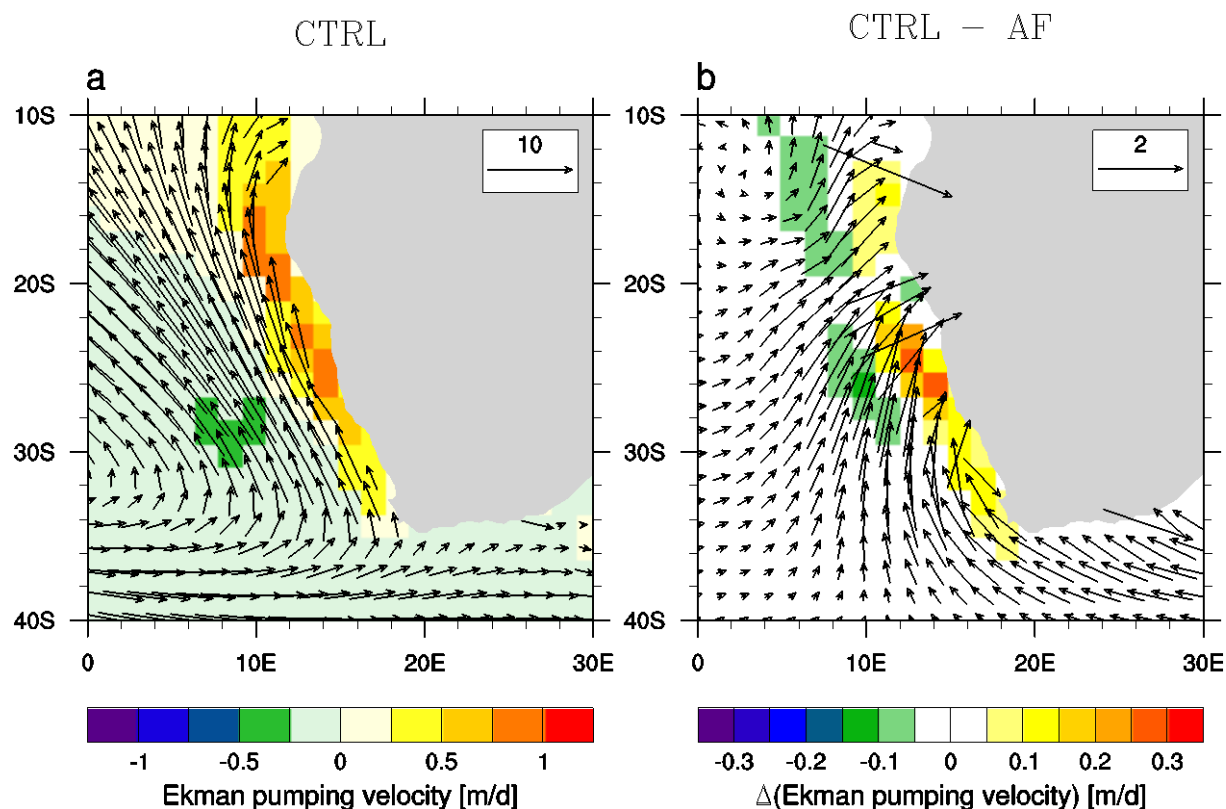
Fig 4: Annual mean surface wind (arrows) [m s⁻¹] and Ekman pumping velocity [m d⁻¹] (shading) for CTRL (a) and response to
10   **African mountain uplift (CTRL – AF) (b). Positive Ekman pumping velocities imply upwelling.**

For the Benguela region, Ekman pumping is already relatively strong with lower mountains, and further increases by about 60%. For the California upwelling region, the average simulated Ekman pumping intensity is rather weak with low mountains and increases by up to 100% with mountain uplift. Here we illustrate only the summer season for the California upwelling region since most intense upwelling activity is found in that season and upwelling is almost absent in autumn and
15   winter.
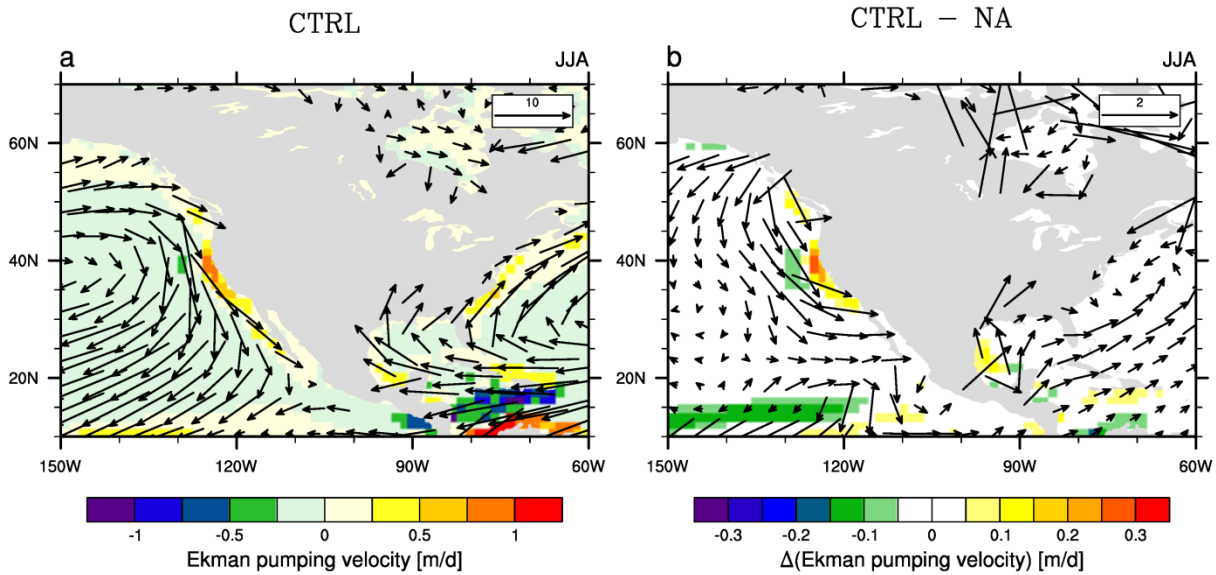
Fig 5: Seasonal mean surface wind (arrows) [m s^{-1}] and Ekman pumping velocity [m d^{-1}] (shading) for CTRL (a) and response to North American mountain uplift (CTRL – NA) (b), both for the summer season (JJA).
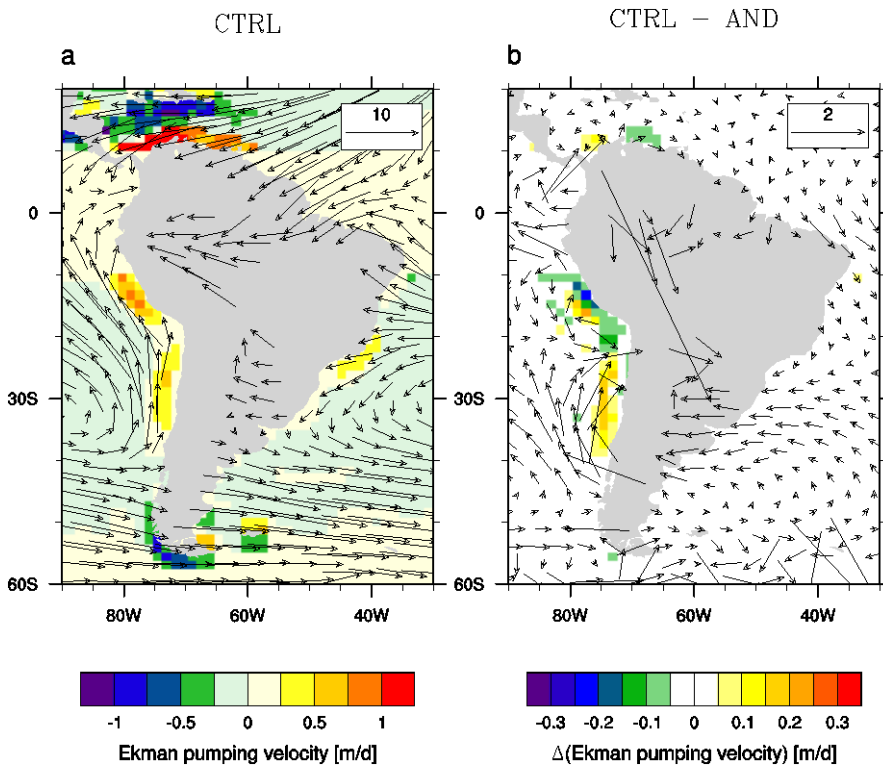
5 **Fig 6: Annual mean surface wind (arrows) [m s^{-1}] and Ekman pumping velocity [m d^{-1}] (shading) for CTRL (a) and response to South American mountain uplift (CTRL – AND) (b).**

For the Andean uplift experiment (Figure 6), the intensification of wind and Ekman pumping occurs mainly south of ~22.5°S in the Chile upwelling region, whereas in the annual mean Ekman pumping, as well as wind stress, north of that latitude, in the Peru upwelling region, decreases. For the Southern Humboldt (Chile upwelling) region we find an intensification of the southerly branch of the South Pacific Anticyclone, leading to increased wind stress and Ekman pumping. But not only the alongshore wind component is strengthened; the wind is also directed more towards the coast.

5.2.2 Upper-ocean temperatures

Considering changes in SSTs (Figure 7) we find that in the Benguela, as well as in the California upwelling region there is a cooling of the upper ocean (up to 2.5 °C and up to 1.5°C, respectively). For the Humboldt Current and upwelling region we find a cooling with uplift in the region north of ~22.5°S despite a decrease in upwelling-favourable winds and Ekman pumping intensities. South of that latitude we observe a warming even though Ekman pumping and low-level winds indicate intensified upwelling.

In the following we examine whether the changes in Ekman pumping velocities, that are driven by surface wind modifications are translated into vertical velocity changes in the oceanic column by the ocean model and whether or not this results in a change in the vertical advective heat flux, that is dominating the temperature signal of the different upwelling regions. To this end we illustrate the temperature response together with the vertical motion change of the model layer with the largest response in upwelling velocity for the respective regions (Figure 8).

In the Benguela region zones with increased upwelling velocity clearly coincide with cooling areas (Figure 8a) down to about 150 m (not shown) with temperature responses reaching over 3°C. This was discussed and illustrated also in Jung et al. (2014). In the California region, the match of the spatial distribution of vertical velocity change and temperature change is not as good as in the Benguela Upwelling System. The best overlap is found mostly during boreal summer (Figure 8b) and autumn seasons (not illustrated), the major upwelling seasons of the California Upwelling System. For the Humboldt region (Figure 8c), this comparison shows that there is no obvious connection between upwelling/vertical heat advection change and temperature change for Andean uplift (neither in the Peru, nor in the Chile upwelling region). Indeed, in the Chile area, despite an increase in upwelling velocities there is a warming of up to 3°C down to over 200 m depth (not shown).
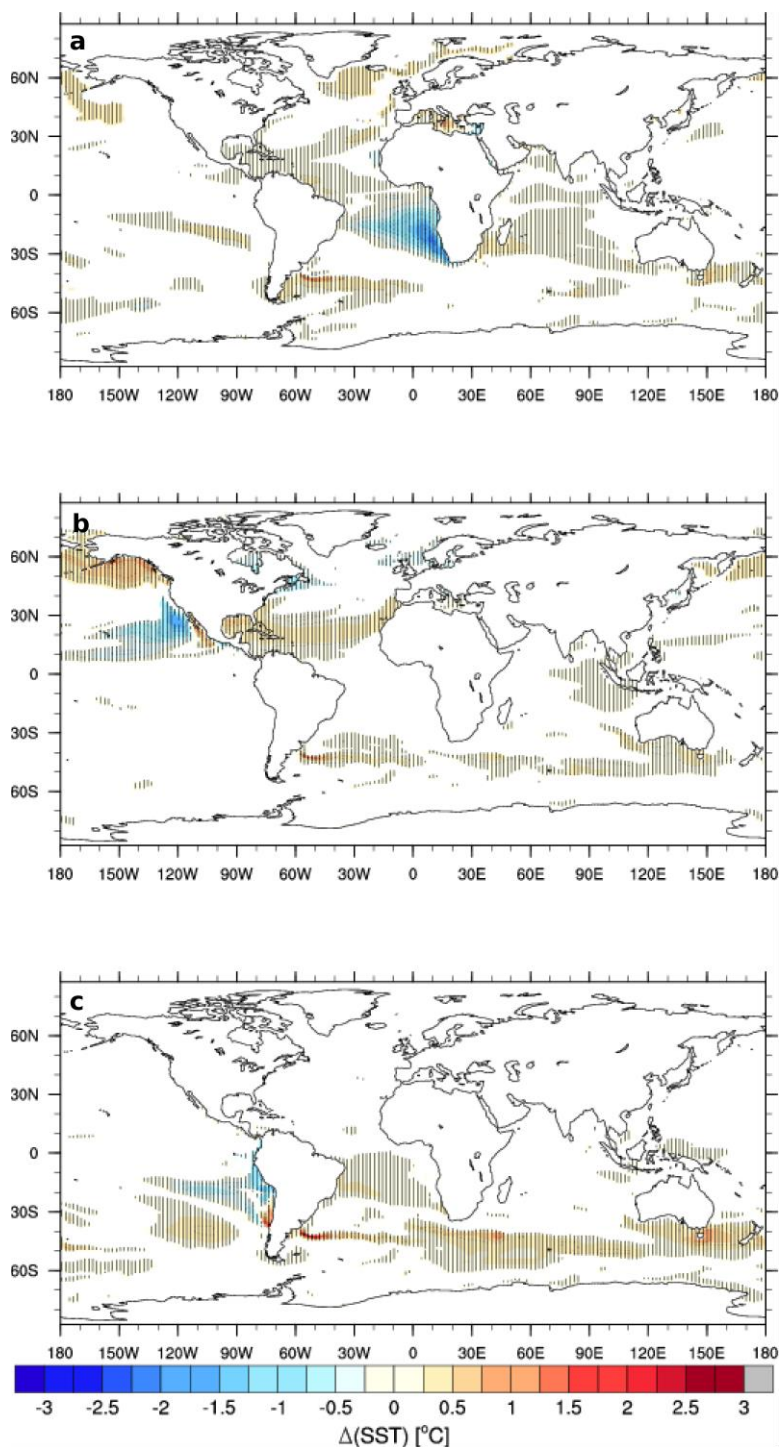
Fig 7: Annual mean SST response [°C] to African mountain uplift (CTRL – AF)(a), North American uplift (CTRL – NA)(b) and Andean uplift (CTRL – AND)(c), regions of high significance according to t-test (p < 0.01) hatched.
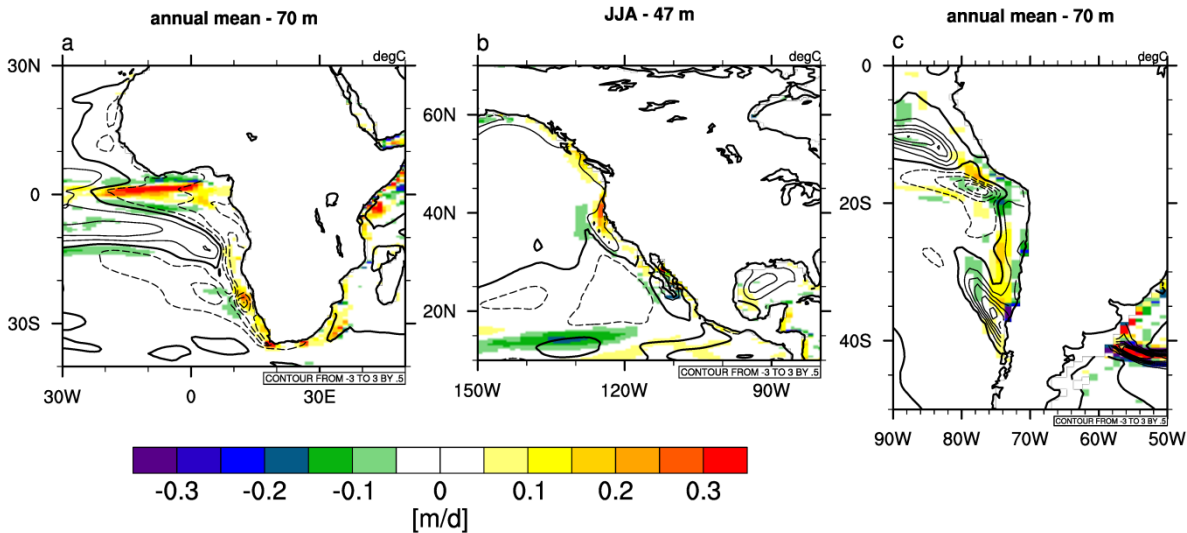
Fig 8: Vertical velocity responses [m d^{-1}] (shading) and temperature responses [°C] (contours) to African (a), North American (b), and South American (c) mountain uplift. For African (a) and South American uplift (c) the annual mean responses are illustrated for 70m depth, whereas for North American uplift (b) the response is illustrated for a depth of 47 m in the upwelling season in boreal summer (JJA).

5.2.3 Vertical velocity and ocean stratification

Even though there is a clear connection between surface wind strength (and direction) and the intensity of oceanic upwelling, an increase in upwelling velocities does not necessarily lead to an upper-ocean cooling. A second ingredient that is needed is a stratified coastal surface ocean. In case of a very small vertical temperature gradient in the upper ocean, even a large increase in upwelling velocities will not lead to a major cooling.

The following figures illustrate vertical cross-sections at the latitude of maximum upwelling velocities in the coastal zones of the investigated upwelling areas. The cross-sections illustrate vertical velocities and temperatures in the simulation with low mountains and the changes of both variables with respect to mountain uplift. To see a clearer relationship, instead of annual means, we show seasonal averages for the seasons with the largest upwelling intensities and upwelling response intensities (i.e. SON for the Chile upwelling area and JJA for the other regions).

As discussed in Jung et al. (2014), in the Benguela region, clearly an intensification of upwelling is found that leads to a significant cooling of the upper ocean that is strongest at a depth of ~50-100 m. Here, the upwelling intensification works in concert with the strongest vertical temperature gradient that is found exactly at this depth (Figure 9).
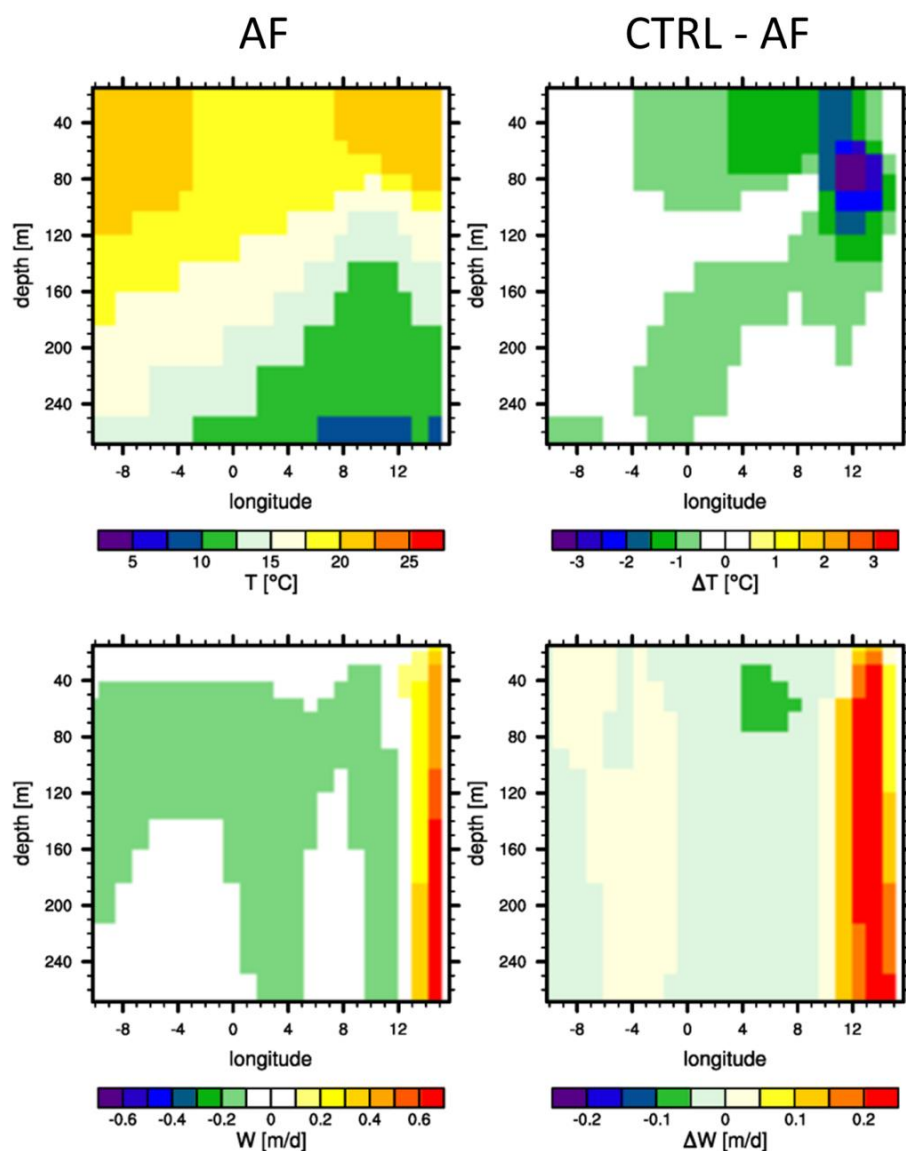
Fig 9: Vertical cross-sections (at ~25°S): seasonal means of temperature (upper left), temperature response to mountain uplift (upper right), vertical oceanic velocity (lower left) and response in upwelling velocity (lower right) for the Benguela upwelling region for boreal summer (JJA).

5   The California upwelling region is characterized by a clear intensification of upwelling velocities, which is shown in a vertical cross-section at 39°N (Figure 10, lower panel). Despite this intensification of upwelling velocity, no cooling signal of the upper ocean is found in the region of maximum upwelling response (Figure 10, upper right panel). This is explained by the weak vertical temperature gradient of the surface ocean in that area (Figure 10, upper left panel). The observed surface cooling that is most prominent south of 30°N is hence most likely not mainly influenced by upwelling intensification

in this model experiment. In case of a more stratified ocean in combination with a stronger upwelling response (which might be the case in a higher resolved model and in reality) this might indeed have a larger contribution to upper-ocean cooling, since it was illustrated that simulated upwelling velocities are underestimated.
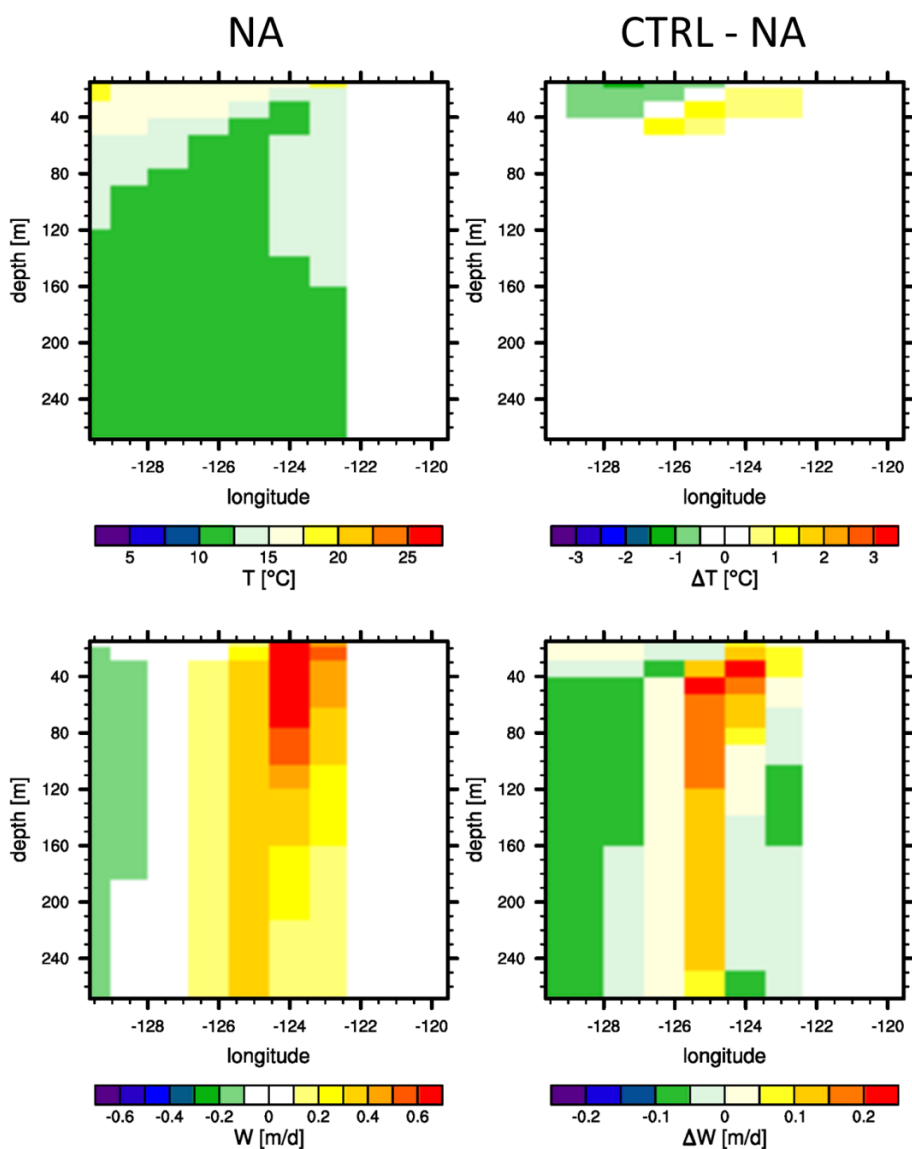
5   **Fig 10: Vertical cross-sections (at ~39°N): seasonal means of temperature (upper left), temperature response to mountain uplift (upper right), vertical oceanic velocity (lower left) and response in upwelling velocity (lower right) for the California upwelling region for boreal summer (JJA).**

In the Peru zone upwelling is evident and we find a small decrease in upwelling intensity in the vicinity of the coast (Figure 11, lower right panel), like it was also evident in Figure 8. Nevertheless we observe a slight surface cooling (Figure 11,

upper right panel), even though the stratification of the surface ocean is not minor. Hence other reasons for the temperature change signal with mountain uplift are to be found.
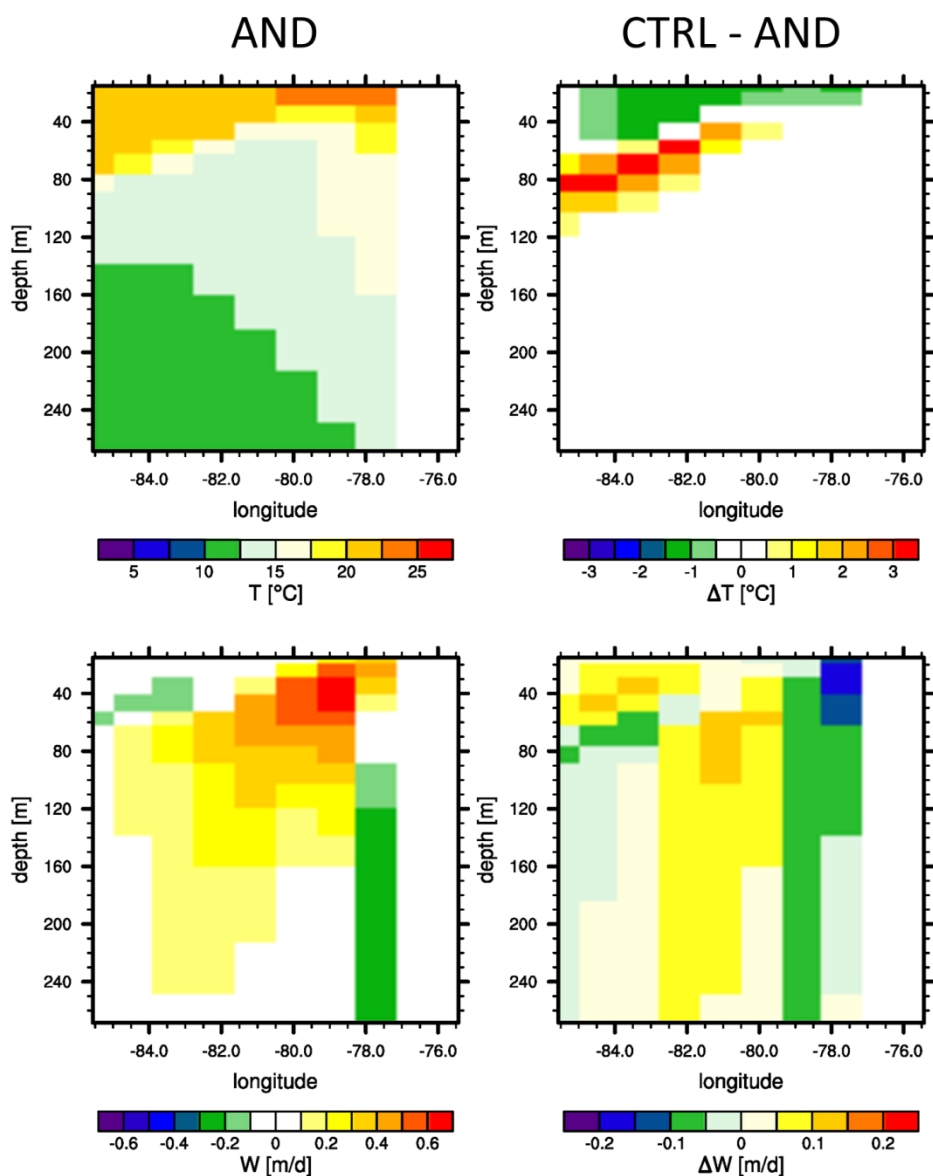
Fig 11: Vertical cross-sections (at ~15°S): seasonal means of temperature (upper left), temperature response to mountain uplift (upper right), vertical oceanic velocity (lower left) and response in upwelling velocity (lower right) for the Northern Humboldt area (Peru upwelling region) for boreal summer (JJA).

In the Southern Humboldt region, upwelling in the major upwelling zone is rather weak in the model representation for boreal fall (SON) with low mountains, but it increases with mountain uplift (Figure 12). What was not evident from the SST warming in Figure 7 is, that there is indeed a response to the upwelling intensification that manifests in a weak cooling signal

at a depth of ~40-80 m. However, upwelling velocities, as well as the ocean stratification are still relatively small with high mountains.
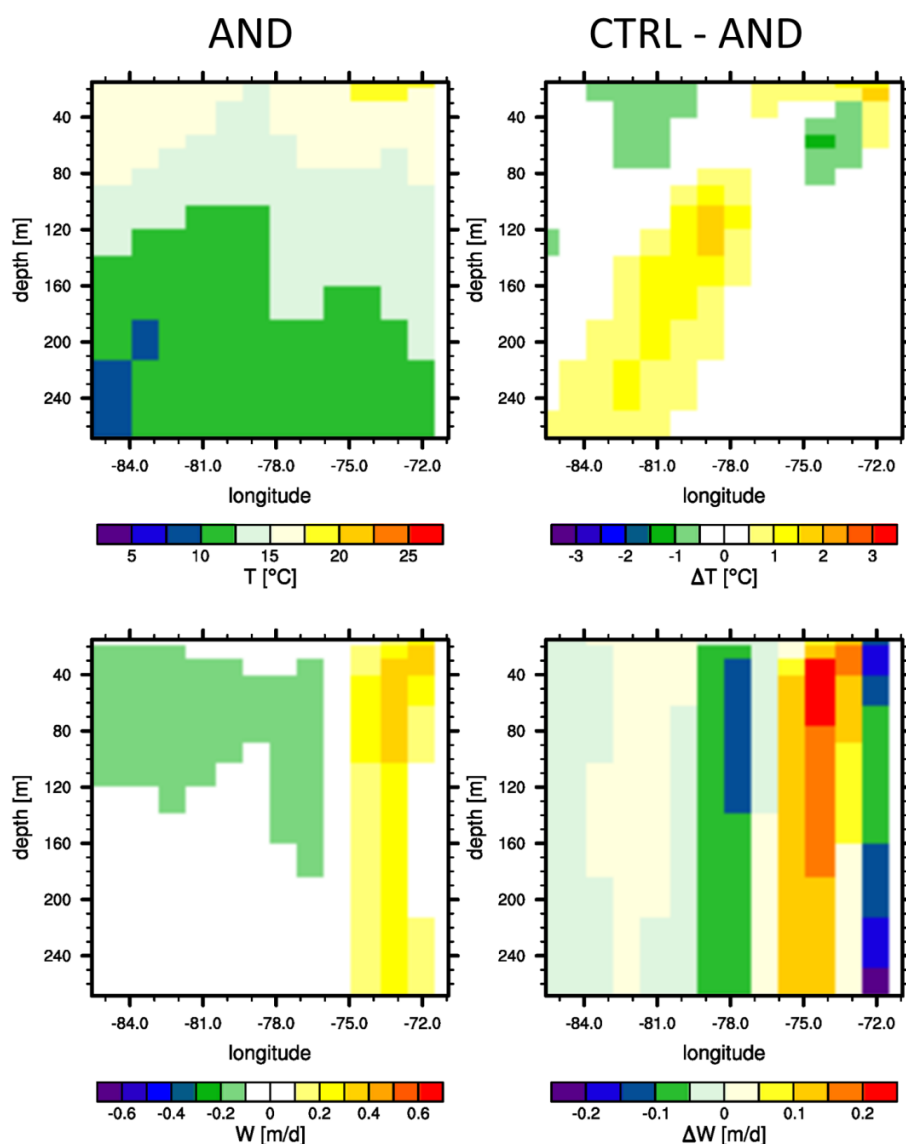
Fig 12: Vertical cross-sections (at ~29°S): seasonal means of temperature (upper left), temperature response to mountain uplift (upper right), vertical oceanic velocity (lower left) and response in upwelling velocity (lower right) for the Southern Humboldt area (Peru upwelling region) for boreal autumn (SON).

Nevertheless there is a warming signal at the surface and further off the coast down to greater depth (max at ~120 m) that is not related to upwelling activity changes and dominates the response in SST. This temperature change maximum (Figure 7)

is found further South (~33°S) than the one illustrated by the cross-section, which is situated at the latitude of maximum upwelling response (~29°S).

5.2.4 Surface heat fluxes and low clouds

Surface heat fluxes are likely to alter SSTs in addition to the changes in upwelling strength, but they are also affected by SST

5 changes and hence play a crucial role in atmosphere-ocean feedbacks. In the following we compare surface heat fluxes and illustrate them with respect to their effect on the oceanic heat content. Hence, a reduced solar radiative flux (directed from the atmosphere to the ocean) would lead to a cooling of the ocean, whereas reduced latent and sensible heat fluxes would contribute to a warming of the ocean and hence be displayed as such.

As illustrated in Figure 13 (and similarly in Jung et al. (2014)), in the Benguela upwelling area, the cooling is mainly

10 determined by vertical advective heat fluxes, whereas the surface heat fluxes approximately cancel out. The latent heat flux to the atmosphere is strongly reduced due to reduced SSTs, contributing to a positive change in the surface ocean heat balance. The changes in net surface radiative heat flux and sensible heat flux are negative. Reasons might be an increase in low cloud coverage and the increase in near-coastal wind strength in combination with increased cold-air advection from the South.
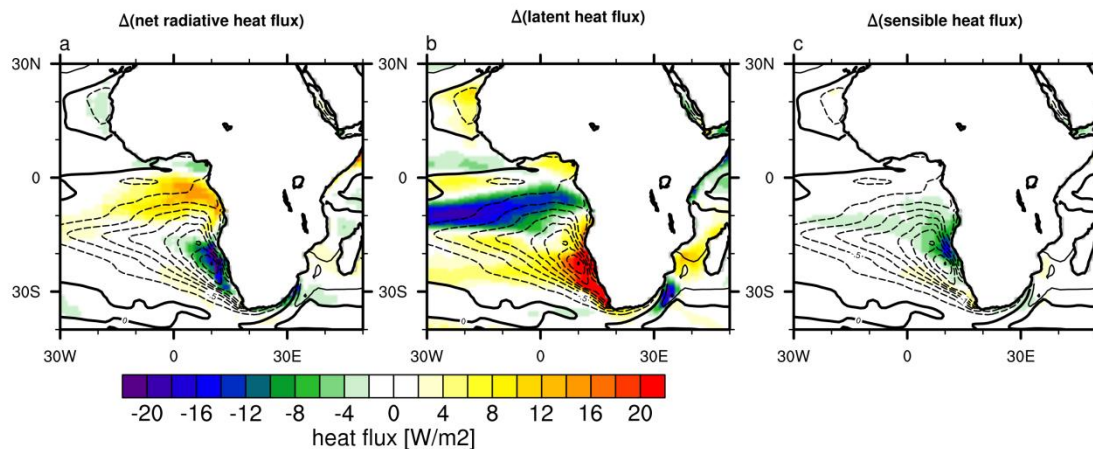
Fig 13: Annual mean responses of surface heat fluxes to African uplift [W m^{-2}]: net radiative heat flux (a), latent heat flux (b), sensible heat flux (c); note: what is illustrated is the effect of the surface heat fluxes on the ocean heat content, contours: SST response (intervals: 0.5°C)

For the California upwelling region (Figure 14), sensible heat flux changes are also relatively weak. Despite the strengthened

20 surface wind, latent heat flux is slightly weakened due to the surface cooling. Net radiative heat influx is strongly decreased due to increased low cloud coverage, as is illustrated below. The net radiative heat flux change is by far the most important contribution of the surface fluxes and hence acts in concert with the rather weak upwelling intensification.
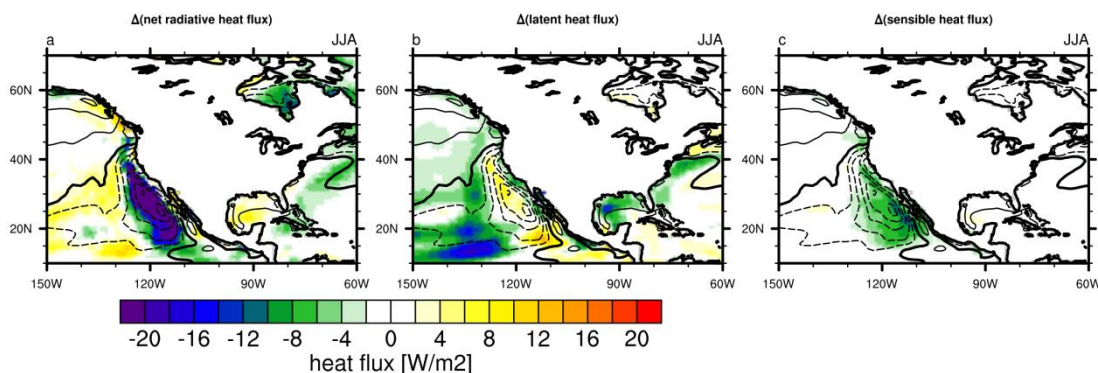
Fig 14: Seasonal mean (JJA) responses of surface heat fluxes to North American uplift [W m⁻²] in boreal summer: net radiative heat flux (a), latent heat flux (b), sensible heat flux (c); note: what is illustrated is the effect of the surface heat fluxes on the ocean heat content, contours: SST response (intervals: 0.5°C)
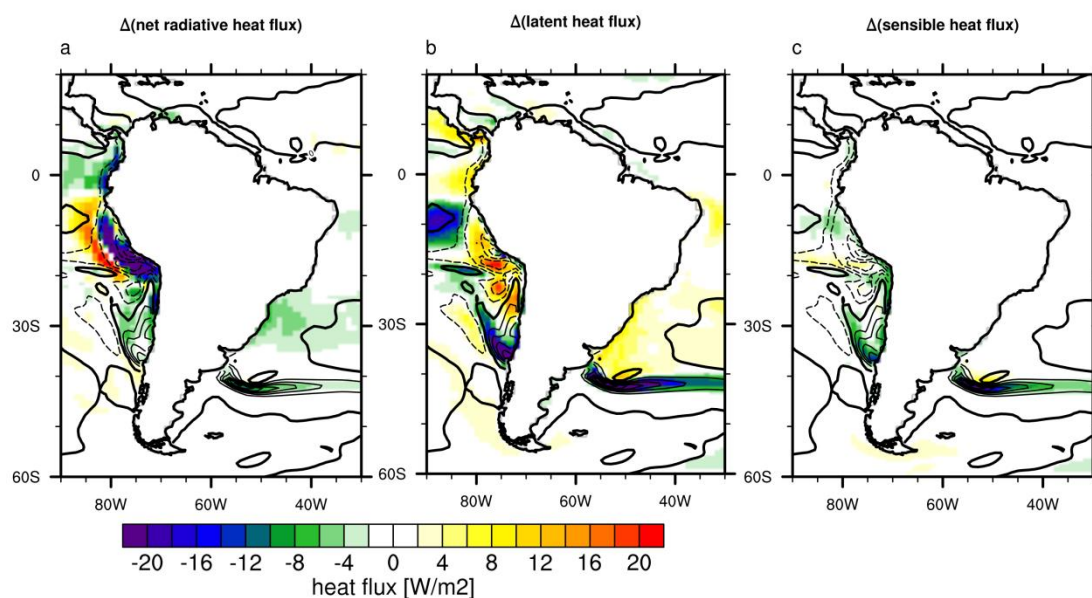
Fig 15: Annual mean responses of surface heat fluxes to Andean uplift [W m⁻²]: net radiative heat flux (a), latent heat flux (b), sensible heat flux (c); note: what is illustrated is the effect of the surface heat fluxes on the ocean heat content, contours: SST response (intervals: 0.5°C)

In the Northern Humboldt region the cloud radiative feedback acts to reduce surface energy balance by altering the net radiative heat flux (Figure 15) and hence opposes the reduction of upwelling which would otherwise lead to a warming of the sea surface. The latent heat flux is reduced, most likely as a consequence of the decrease in surface winds and of surface cooling and hence counteracts the overall cooling. Sensible heat flux changes are small for the Northern Humboldt region (and of different sign) and therefore have a negligible effect on SSTs. From this analysis it appears that the strongest effect of mountain uplift works via the net radiative heat flux, leading to a cooling, despite a reduction in upwelling and the

contrary effect of latent heat flux. This reduction of the net radiative heat flux is mainly caused by an increase in cloud coverage, which will be discussed in the following.

In the Southern Humboldt region both, net radiative and sensible heat flux are not of major importance for SST change, whereas the latent heat flux is strongly increased (indicated by a negative contribution to the surface heat balance of the

5   ocean). Most likely this effect is caused by the increase in SST and the intensification of the wind strength. All components of the surface heat balance indicate a cooling in the Southern Humboldt region and are hence acting in concert with upwelling intensification. Therefore other explanations are needed for the strong warming of the surface ocean that can be observed in the Southern Humboldt upwelling area.

In three of the upwelling areas, namely the Peru, Benguela and California upwelling zones we could identify a strong

10   decrease in net radiative heat flux. This net radiative heat flux response is to a major part caused by an increase in low cloud coverage that is illustrated in Figure 16a-c for the different experiments. Model experiments for South America and Africa (Richter and Mechoso, 2006, 2004;Feng and Poulsen, 2014) showed that elevated terrain acts on lower tropospheric stability, resulting in an increase of low cloud coverage off the coast. This is caused by the blocking and deflection of the Westerlies (for South America additionally a blocking of the North-Easterly flow) which leads to subsidence warming above the

15   planetary boundary layer and cold-air advection within the planetary boundary layer. This increase in cloud coverage already occurs in the studies without coupled ocean (Richter and Mechoso, 2006, 2004), but the effect is most likely strengthened by atmosphere-ocean feedback mechanisms, since the increased cloud coverage leads to a sea surface cooling due to reduction of incoming solar radiation which then leads to an enhanced cooling in the lower layers of the atmosphere which further enhances the effect on tropospheric stability and low-level cloud coverage, forming a positive feedback loop.
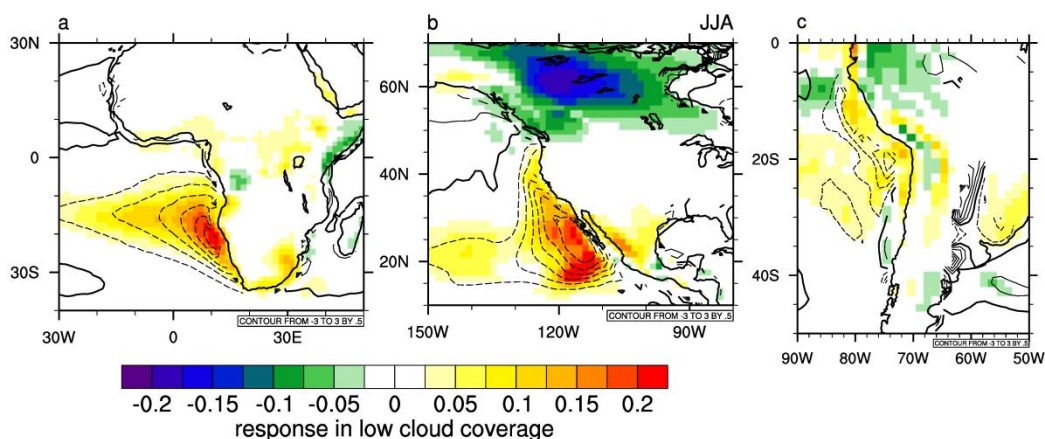
Fig 16: Responses in low cloud coverage (shading) and temperature (contours, intervals: 0.5°C) to African (CTRL – AF)(a), North American (CTRL – NA)(b), and South American (CTRL – AND)(c) mountain uplift. For African (a) and South American uplift (c) the annual mean responses are illustrated, whereas for North American uplift (b) the response is illustrated for the upwelling season in boreal summer (JJA).

5.2.5 Horizontal heat advection in the surface ocean

Another important factor related to oceanic temperature evolution is the influence of horizontal heat transports. In the Benguela region (Figures 17a and 17d), there is mainly a strengthening of northwestward current velocities and hence advection of colder waters from the Southeast occurs. The flow pattern also indicates that the cooling signal is mainly connected to the region of maximum upwelling intensification and is eventually transported with the prevailing flow pattern. The cooling is additionally intensified by the increase in the transport of cooler waters from the South.
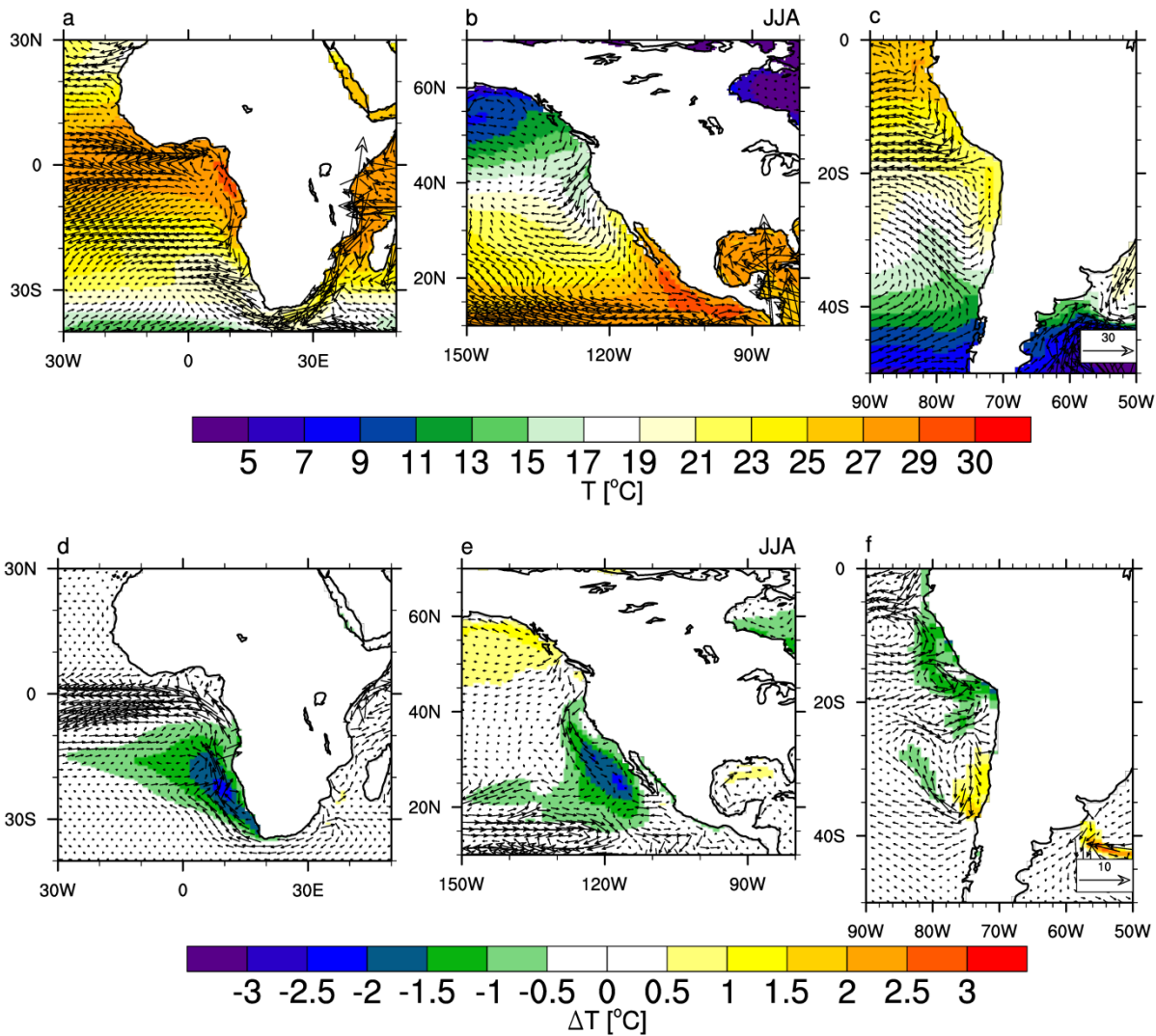
Fig. 17: Surface (first model layer) horizontal velocity [m s⁻¹](vectors) and SST [°C](shading) for CTRL (a,b,c); horizontal velocity responses [m s⁻¹] (vectors) and temperature responses [°C] (shading) to African (CTRL – AF)(d), North American (CTRL – NA)(e), and South American (CTRL – AND)(f) mountain uplift. For Africa (a,d) and South America (c,f) the annual means are illustrated, whereas for North America (b,d) the seasonal mean in the upwelling season in boreal summer (JJA) is shown.

In the California region (Figures 17b and 17e), the strong cooling signal seems to be most likely related to the strengthening of the southward transport of cool water masses. Here, the strongest cooling signal is not found in the area, where we see the strongest upwelling intensification (Figure 8), but further to the South, where the southward flow intensification ceases and turns into a slight southward flow decrease. This indicates that in contrast to the Benguela upwelling region, upwelling does not play an as important role for upper-ocean cooling, whereas horizontal heat transport is more important.

For the Peru upwelling zone (Figures 17c and 17f) there seems to be no direct connection between the transport of water masses and SST, since the horizontal temperature gradient in that area is very small.

In the Chile upwelling zone (Figures 17c and 17f), where surface energy fluxes, as well as upwelling intensities did not show any relation to the strong upper-ocean warming, we can clearly relate the temperature changes to an intensification of the Peru-Chile undercurrent and of the Peru-Chile countercurrent. This southward flow anomaly is most likely related to changes in wind stress curl and associated Sverdrup dynamics (Karstensen and Ulloa, 2009). As illustrated in the cross-section in Figure 12, also an upwelling-induced small cooling signal is found in the sub-surface, but this is overlain by this very strong transport of warm water masses from the North to the South.

6 Discussion

Dekens et al. (2007) suggested that the long-term cooling trends, which are obvious in all major EBUSs since at least the Pliocene, are attributable to factors like changes in depth and/or temperature of the thermocline. Even though these factors might have played a role (Steph et al., 2010) our study suggests that mountain uplift processes need also to be considered as a possible cause for the cooling in some of the EBUSs.

Not many studies were performed so far, analysing the effect of mountain uplift on atmospheric and oceanic dynamics with a coupled global general circulation model. Jung et al. (2014, 2016) illustrated how African topography shaped atmospheric circulation patterns that have a strong influence on the strength of the Benguela Upwelling System, but also on precipitation and vegetation cover. Sepulchre et al. (2009) investigated the influence of Andean uplift on the Humboldt Current. They found rather similar results regarding the atmospheric response with their uncoupled atmosphere general circulation model (AGCM). The oceanic response comparing our coupled model to their offline used regional ocean circulation model ROMS shows large differences, most likely caused by missing feedback mechanisms and the higher resolution of the regional ocean model. A model study, applying the relatively highly resolved atmosphere-only GCM CAM5 for present-day and Pliocene topography (globally) to investigate the effects of uplift on the worlds' major upwelling regimes showed similar results in terms of the cloud-radiative response to mountain uplift (Arnold and Tziperman, 2016). Potter et al. (2017) compared a low resolution atmosphere-only and a coupled model for the response to Andean uplift. Their simulation also showed an increased low cloud formation with high mountains and a much reduced cloud coverage in the low mountains scenario. The low cloud reduction is stronger in the non-coupled simulation, but extends further West over the ocean in the coupled simulation, due to atmosphere-ocean feedbacks and dynamic ocean processes, as well as model deficiencies. A coupled

global circulation model (CCSM4) was used by Feng and Poulsen (2014) to investigate the effect of Andean uplift on atmosphere and ocean. The study showed similar results than our simulations in terms of clouds, surface wind, SST and also horizontal heat advection in a simulation with flat Andes compared to present-day orography. Another experiment with moderate half Andean elevation resulted in only minor responses. The main difference between their study and the present

5 investigation is, that they did not show a contradictory effect for the Peru and the Chile upwelling areas, which might well be related to the fact that in their experiment Andean topography was completely flat. The similarity of the different studies underlines the robustness of our findings.
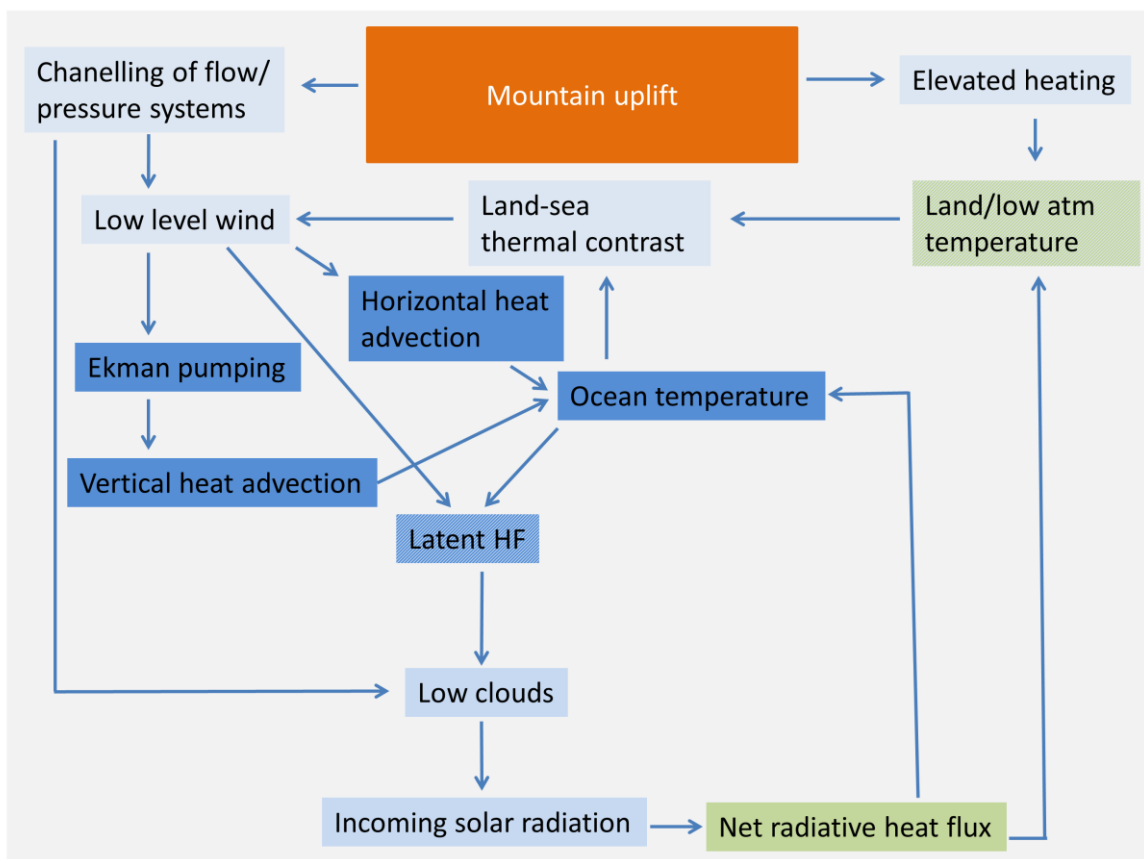
Fig. 18: Summary of relevant processes interacting in case of continental-scale mountain uplift considered in this study. The
10 **complexity of the processes lead to negative, as well as positive feedback mechanisms that also depend on the regions'**
characteristics. Colors: light blue – atmospheric processes, blue – oceanic processes, green – land surface related processes,
orange – forcing (i.e. mountain uplift).

Figure 18 illustrates the most important processes that were analysed in this study and that play a role in the responses of EBUSs to continental-scale mountain uplift. Mountain uplift on one hand leads to elevated heating which then results in a

15 strengthened land-ocean temperature gradient in the lower atmosphere, which through thermal wind relation leads to intensified low-level jets that are the main drivers of upwelling in EBUSs. Additionally, higher mountains directly affect the

low- level winds near the coast by a channelling of the flow. However, the low-level winds do not only affect upwelling activity, but also act on horizontal heat transport which might lead to either a warming, or a cooling of upper-ocean temperatures. Low-level winds, as well as ocean temperatures act on the latent heat flux which is an ingredient for the formation of low clouds. More importantly low cloud coverage is influenced by mountains due to blocking of westerly flow

5 and an increase in lower tropospheric stability, as described in detail by Richter and Mechoso (2006, 2004). The increase in low cloud coverage reduces downward shortwave radiation, and hence the net radiative heat flux, leading to an additional cooling of the sea surface. The resulting SSTs then also form part of the atmosphere-ocean feedback in EBUS, as described in Nicholson (2010) for the Benguela upwelling region.

7 Summary and Conclusions

10 In almost all studied regions with coastal mountains and prevailing coastal parallel winds (Benguela, California and Southern Humboldt), we find intensified low-level winds, and an intensification of Ekman pumping velocities with mountain uplift, most likely related to the thermal wind relationship, following elevated heating, as explained in Jung et al. (2014).

To which extent this leads to SST cooling depends on a variety of influencing factors and feedback mechanisms that differ for the different upwelling regions.

15 • Benguela region: the coastal low-level jet and Ekman pumping intensification are the dominant factors in controlling the SST response, but horizontal heat advection also contributes to upper-ocean cooling.

• California region: the coastal low-level jet and Ekman pumping intensify during the summer season, but horizontal heat advection, as well as the net radiative effect due to an increased low cloud coverage are likely more important for SST cooling.

20 • Humboldt region: the weak ocean stratification hinders SST response to changing upwelling velocities. In the Chile upwelling area horizontal heat advection is dominant. Upper-ocean warming is observed, despite an intensified coastal low-level jet and strengthened upwelling activity. In the Peru upwelling zone the net radiative cooling effect is dominant, which is also caused by a low-level cloud coverage increase.

It could be demonstrated, that mountain uplift is important for upper-ocean temperature evolution in the area of Eastern

25 Boundary Currents. The relative importance of the different feedbacks and processes depends on the upwelling region (e.g. mountain elevation, ocean stratification), but might also be influenced by model resolution, since the response of upwelling to low-level wind intensification in a global GCM is limited and most likely underestimated.

Author contributions

Gerlinde Jung and Matthias Prange designed the experiments. Gerlinde Jung set up the model, performed the simulations
30 and the output analysis and prepared the manuscript with contributions from Matthias Prange.

Acknowledgements

This work was funded by the Deutsche Forschungsgemeinschaft (DFG) Research Center/Excellence Cluster "The Ocean in the Earth System".

The authors like to thank Gary Strand of NCAR for making available the spun-up preindustrial control run restart files and

5   Matthew Hecht from the Los Alamos National Lab for his assistance with the production of mapping files for this model version. Thanks to Bruce Briegleb (NCAR) for making pre-industrial aerosol data available.

The CCSM3 experiments were run on the SGI Altix Supercomputer of the "Norddeutscher Verbund für Hoch- und Höchstleistungsrechnen" (HLRN). Model setup and output analysis and plotting was performed using cran R (R-Development-Core-Team, 2011) and NCL software.

10   **References**

Arnold, N. P., and Tziperman, E.: Reductions in midlatitude upwelling-favorable winds implied by weaker large-scale pliocene sst gradients, Paleoceanography, 31, 27-39, 10.1002/2015PA002806, 2016.

Barnes, J. B., Ehlers, T. A., Insel, N., McQuarrie, N., and Poulsen, C. J.: Linking orography, climate, and exhumation across the central andes, Geology, 40, 1135-1138, Doi 10.1130/G33229.1, 2012.

15   Belmadani, A., Echevin, V., Codron, F., Takahashi, K., and Junquas, C.: What dynamics drive future wind scenarios for coastal upwelling off peru and chile?, Climate Dynamics, 43, 1893-1914, DOI 10.1007/s00382-013-2015-2, 2014.

Bergh, E. W., Compton, J. S., and Frenzel, P.: Late neogene foraminifera from the northern namibian continental shelf and the transition to the benguela upwelling system, J Afr Earth Sci, 141, 33-48, 10.1016/j.jafrearsci.2018.01.018, 2018.

Bissig, T., and Riquelme, R.: Andean uplift and climate evolution in the southern atacama desert deduced from

20   geomorphology and supergene alunite-group minerals, Earth and Planetary Science Letters, 299, 447-457, DOI 10.1016/j.epsl.2010.09.028, 2010.

Blisniuk, P. M., Stern, L. A., Chamberlain, C. P., Idleman, B., and Zeitler, P. K.: Climatic and ecologic changes during miocene surface uplift in the southern patagonian andes, Earth and Planetary Science Letters, 230, 125-142, 10.1016/j.epsl.2004.11.015, 2005.

25   Bonan, G. B., Levis, S., Sitch, S., Vertenstein, M., and Oleson, K. W.: A dynamic global vegetation model for use with climate models: Concepts and description of simulated vegetation dynamics, Global Change Biol, 9, 1543-1566, DOI 10.1046/j.1365-2486.2003.00681.x, 2003.

Braconnot, P., Otto-Bliesner, B., Harrison, S., Joussaume, S., Peterchmitt, J. Y., Abe-Ouchi, A., Crucifix, M., Driesschaert, E., Fichefet, T., Hewitt, C. D., Kageyama, M., Kitoh, A., Laine, A., Loutre, M. F., Marti, O., Merkel, U., Ramstein, G.,

30   Valdes, P., Weber, S. L., Yu, Y., and Zhao, Y.: Results of pmip2 coupled simulations of the mid-holocene and last glacial maximum - part 1: Experiments and large-scale features, Climate of the Past, 3, 261-277, 2007.

Burk, S. D., and Thompson, W. T.: The summertime low-level jet and marine boundary layer structure along the california coast, Monthly Weather Review, 124, 668-686, 1996.

Chavez, F. P., and Messie, M.: A comparison of eastern boundary upwelling ecosystems, Prog Oceanogr, 83, 80-96, DOI 10.1016/j.pocean.2009.07.032, 2009.

5   Checkley, D. M., and Barth, J. A.: Patterns and processes in the california current system, Prog Oceanogr, 83, 49-64, DOI 10.1016/j.pocean.2009.07.028, 2009.

Clarke, J. D. A.: Antiquity of aridity in the chilean atacama desert, Geomorphology, 73, 101-114, 10.1016/j.geomorph.2005.06.008, 2006.

Collins, W. D., Bitz, C. M., Blackmon, M. L., Bonan, G. B., Bretherton, C. S., Carton, J. A., Chang, P., Doney, S. C., Hack,
10   J. J., Henderson, T. B., Kiehl, J. T., Large, W. G., McKenna, D. S., Santer, B. D., and Smith, R. D.: The community climate system model version 3 (ccsm3), Journal of Climate, 19, 2122-2143, 2006.

Dekens, P. S., Ravelo, A. C., and McCarthy, M. D.: Warm upwelling regions in the pliocene warm period, Paleoceanography, 22, PA3211, 2007.

Doyle, J. D.: The influence of mesoscale orography on a coastal jet and rainband, Monthly Weather Review, 125, 1465-
15   1488, Doi 10.1175/1520-0493(1997)125<1465:Tiomoo>2.0.Co;2, 1997.

Dupont, L. M., Rommerskirchen, F., Mollenhauer, G., and Schefuß, E.: Miocene to pliocene changes in south african hydrology and vegetation in relation to the expansion of c-4 plants, Earth and Planetary Science Letters, 375, 408-417, 10.1016/j.epsl.2013.06.005, 2013.

Ehlers, T. A., and Poulsen, C. J.: Influence of andean uplift on climate and paleoaltimetry estimates, Earth and Planetary
20   Science Letters, 281, 238-248, DOI 10.1016/j.epsl.2009.02.026, 2009.

Feng, R., and Poulsen, C. J.: Andean elevation control on tropical pacific climate and enso, Paleoceanography, 29, 795-809, Doi 10.1002/2014pa002640, 2014.

Foster, G. L., Lunt, D. J., and Parrish, R. R.: Mountain uplift and the glaciation of north america - a sensitivity study, Climate of the Past, 6, 707-717, 10.5194/cp-6-707-2010, 2010.

25   Garcia-Reyes, M., and Largier, J. L.: Seasonality of coastal upwelling off central and northern california: New insights, including temporal and spatial variability, J Geophys Res-Oceans, 117, Doi 10.1029/2011jc007629, 2012.

Garreaud, R. D., and Munoz, R. C.: The low-level jet off the west coast of subtropical south america: Structure and variability, Monthly Weather Review, 133, 2246-2261, Doi 10.1175/Mwr2972.1, 2005.

Garzione, C. N., Molnar, P., Libarkin, J. C., and MacFadden, B. J.: Rapid late miocene rise of the bolivian altiplano:
30   Evidence for removal of mantle lithosphere, Earth and Planetary Science Letters, 241, 543-556, 10.1016/j.epsl.2005.11.026, 2006.

Ghosh, P., Garzione, C. N., and Eiler, J. M.: Rapid uplift of the altiplano revealed through c-13-o-18 bonds in paleosol carbonates, Science, 311, 511-515, 10.1126/science.1119365, 2006.

Gregory-Wodzicki, K. M.: Uplift history of the central and northern andes: A review, Geol Soc Am Bull, 112, 1091-1105, Doi 10.1130/0016-7606(2000)112<1091:Uhotca>2.3.Co;2, 2000.

Grimmer, F., Dupont, L., Lamy, F., Jung, G., Gonzalez, C., and Wefer, G.: Early pliocene vegetation and hydrology changes in western equatorial south america, Climate of the Past, 14, 1739-1754, 10.5194/cp-14-1739-2018, 2018.

Handiani, D., Paul, A., Prange, M., Merkel, U., Dupont, L., and Zhang, X.: Tropical vegetation response to heinrich event 1 as simulated with the uvic escm and ccsm3, Climate of the Past, 9, 1683-1696, DOI 10.5194/cp-9-1683-2013, 2013.

Haskell, W. Z., Hammond, D. E., and Prokopenko, M. G.: A dual-tracer approach to estimate upwelling velocity in coastal southern california, Earth and Planetary Science Letters, 422, 138-149, 10.1016/j.epsl.2015.04.015, 2015a.

Haskell, W. Z., Kadko, D., Hammond, D. E., Knapp, A. N., Prokopenko, M. G., Berelson, W. M., and Capone, D. G.: Upwelling velocity and eddy diffusivity from be-7 measurements used to compare vertical nutrient flux to export poc flux in the eastern tropical south pacific, Mar Chem, 168, 140-150, 10.1016/j.marchem.2014.10.004, 2015b.

Hoetzel, S., Dupont, L. M., and Wefer, G.: Miocene-pliocene vegetation change in south-western africa (odp site 1081, offshore namibia), Palaeogeogr Palaeocl, 423, 102-108, 10.1016/j.palaeo.2015.02.002, 2015.

Holt, T. R.: Mesoscale forcing of a boundary layer jet along the california coast, Journal of Geophysical Research-Atmospheres, 101, 4235-4254, 1996.

Hutchings, L., van der Lingen, C. D., Shannon, L. J., Crawford, R. J. M., Verheye, H. M. S., Bartholomae, C. H., van der Plas, A. K., Louw, D., Kreiner, A., Ostrowski, M., Fidel, Q., Barlow, R. G., Lamont, T., Coetzee, J., Shillington, F., Veitch, J., Currie, J. C., and Monteiro, P. M. S.: The benguela current: An ecosystem of four components, Prog Oceanogr, 83, 15-32, DOI 10.1016/j.pocean.2009.07.046, 2009.

Jung, G., Prange, M., and Schulz, M.: Uplift of africa as a potential cause for neogene intensification of the benguela upwelling system, Nature Geoscience, 7, 741-747, Doi 10.1038/Ngeo2249, 2014.

Jung, G., Prange, M., and Schulz, M.: Influence of topography on tropical african vegetation coverage, Climate Dynamics, 46, 2535-2549, 10.1007/s00382-015-2716-9, 2016.

Karstensen, J., and Ulloa, O.: Peru-chile current system, in: Ocean currents, edited by: Steele, J., Thorpe, S., and Turekian, K., Academic Press, 647 2009.

Keller, G., Adatte, T., Hollis, C., Ordonez, M., Zambrano, I., Jimenez, N., Stinnesbeck, W., Aleman, A., and HaleErlich, W.: The cretaceous/tertiary boundary event in ecuador: Reduced biotic effects due to eastern boundary current setting, Mar Micropaleontol, 31, 97-133, Doi 10.1016/S0377-8398(96)00061-8, 1997.

Levis, S., Bonan, G., Vertenstein, M., and Oleson, K.: The community land model's dynamic global vegetation model (clm-dgvm): Technical description and user's guide, NCAR Tech. Note TN-459+ IA, 50, 2004.

Marlow, J. R., Lange, C. B., Wefer, G., and Rosell-Mele, A.: Upwelling intensification as part of the pliocene-pleistocene climate transition, Science, 290, 2288-2291, 2000.

Montecino, V., and Lange, C. B.: The humboldt current system: Ecosystem components and processes, fisheries, and sediment studies, Prog Oceanogr, 83, 65-79, DOI 10.1016/j.pocean.2009.07.041, 2009.

Montgomery, D. R.: Compressional uplift in the central california coast ranges, Geology, 21, 543-546, Doi 10.1130/0091-7613(1993)021<0543:Cuitcc>2.3.Co;2, 1993.

Moucha, R., and Forte, A. M.: Changes in african topography driven by mantle convection, Nature Geoscience, 4, 707-712, 2011.

5   Mulch, A., Uba, C. E., Strecker, M. R., Schoenberg, R., and Chamberlain, C. P.: Late miocene climate variability and surface elevation in the central andes, Earth and Planetary Science Letters, 290, 173-182, 2010.

Munoz, R. C., and Garreaud, R. D.: Dynamics of the low-level jet off the west coast of subtropical south america, Monthly Weather Review, 133, 3661-3677, Doi 10.1175/Mwr3074.1, 2005.

Nicholson, S. E.: A low-level jet along the benguela coast, an integral part of the benguela current ecosystem, Climatic
10   Change, 99, 613-624, 2010.

Nyblade, A. A., and Robinson, S. W.: The african superswell, Geophysical Research Letters, 21, 765-768, 1994.

Oleson, K. W., Niu, G. Y., Yang, Z. L., Lawrence, D. M., Thornton, P. E., Lawrence, P. J., Stockli, R., Dickinson, R. E., Bonan, G. B., Levis, S., Dai, A., and Qian, T.: Improvements to the community land model and their impact on the hydrological cycle, J Geophys Res-Biogeo, 113, G01021, 2008.

15   Page, B. M., Thompson, G. A., and Coleman, R. G.: Overview: Late cenozoic tectonics of the central and southern coast ranges of california (vol 110, pg 846, 1998), Geol Soc Am Bull, 111, 790-790, 1999.

Parish, T. R.: Forcing of the summertime low-level jet along the california coast, Journal of Applied Meteorology, 39, 2421-2433, Doi 10.1175/1520-0450(2000)039<2421:Fotsll>2.0.Co;2, 2000.

Pickett, M. H., and Paduan, J. D.: Ekman transport and pumping in the california current based on the u.S. Navy's high-
20   resolution atmospheric model (coamps), J Geophys Res-Oceans, 108, 10.1029/2003jc001902, 2003.

Pik, R.: East africa on the rise, Nature Geoscience, 4, 660-661, 2011.

Potter, P. E., and Szatmari, P.: Global miocene tectonics and the modern world, Earth-Sci Rev, 96, 279-295, DOI 10.1016/j.earscirev.2009.07.003, 2009.

Potter, S. F., Dawson, E. J., and Frierson, D. M. W.: Southern african orography impacts on low clouds and the atlantic itcz
25   in a coupled model, Geophysical Research Letters, 44, 3283-3289, 10.1002/2017GL073098, 2017.

R-Development-Core-Team: A language and environment for statistical computing. R foundation for statistical computing. R foundation for statistical computing. Vienna, austria., 2011.

Rachmayani, R., Prange, M., and Schulz, M.: North african vegetation–precipitation feedback in early and mid-holocene climate simulations with ccsm3-dgvm Climate of the Past, 11, 175-185, 2015.

30   Renault, L., Dewitte, B., Falvey, M., Garreaud, R., Echevin, V., and Bonjean, F.: Impact of atmospheric coastal jet off central chile on sea surface temperature from satellite observations (2000-2007), J Geophys Res-Oceans, 114, Doi 10.1029/2008jc005083, 2009.

Richter, I., and Mechoso, C. R.: Orographic influences on the annual cycle of namibian stratocumulus clouds, Geophysical Research Letters, 31, 10.1029/2004gl020814, 2004.

Richter, I., and Mechoso, C. R.: Orographic influences on subtropical stratocumulus, Journal of the Atmospheric Sciences, 63, 2585-2601, Doi 10.1175/Jas3756.1, 2006.

Roberts, E. M., Stevens, N. J., O'Connor, P. M., Dirks, P. H. G. M., Gottfried, M. D., Clyde, W. C., Armstrong, R. A., Kemp, A. I. S., and Hemming, S.: Initiation of the western branch of the east african rift coeval with the eastern branch, Nature Geoscience, 5, 289-294, 2012.

Roberts, G. G., and White, N.: Estimating uplift rate histories from river profiles using african examples, J Geophys Res-Sol Ea, 115, B02406, 2010.

Rommerskirchen, F., Condon, T., Mollenhauer, G., Dupont, L., and Schefuss, E.: Miocene to pliocene development of surface and subsurface temperatures in the benguela current system, Paleoceanography, 26, PA3216, 2011.

Rouault, M., Florenchie, P., Fauchereau, N., and Reason, C. J. C.: South east tropical atlantic warm events and southern african rainfall, Geophysical Research Letters, 30, Artn 8009 Doi 10.1029/2002gl014840, 2003.

Scotese, C. R.: Continental drift:(0-750 million years), PALEOMAP Project, 1998.

Sepulchre, P., Ramstein, G., Fluteau, F., Schuster, M., Tiercelin, J. J., and Brunet, M.: Tectonic uplift and eastern africa aridification, Science, 313, 1419-1423, 2006.

Sepulchre, P., Sloan, L. C., Snyder, M., and Fiechter, J.: Impacts of andean uplift on the humboldt current system: A climate model sensitivity study, Paleoceanography, 24, PA4215, 2009.

Seranne, M., and Anka, Z.: South atlantic continental margins of africa: A comparison of the tectonic vs climate interplay on the evolution of equatorial west africa and sw africa margins, J Afr Earth Sci, 43, 283-300, 2005.

Steph, S., Tiedemann, R., Prange, M., Groeneveld, J., Schulz, M., Timmermann, A., Nurnberg, D., Ruhlemann, C., Saukel, C., and Haug, G. H.: Early pliocene increase in thermohaline overturning: A precondition for the development of the modern equatorial pacific cold tongue, Paleoceanography, 25, 10.1029/2008pa001645, 2010.

Strecker, M. R., Alonso, R. N., Bookhagen, B., Carrapa, B., Hilley, G. E., Sobel, E. R., and Trauth, M. H.: Tectonics and climate of the southern central andes, Annu Rev Earth Pl Sc, 35, 747-787, DOI 10.1146/annurev.earth.35.031306.140158, 2007.

White, L. D., Garrison, R. E., and Barron, J. A.: Miocene intensification of upwelling along the california margin as recorded in siliceous facies of the monterey formation and offshore dsdp sites, in: Upwelling systems: Evolution since the early miocene, edited by: Summerhayes, C. P., Prell, W. L., and Emeis, K. C., Geological Society Special Publication, 429-442, 1992.